Separation Science and Technology
Publication details, including instructions for authors and subscription information:
http://www.informaworld.com/smpp/title~content=t713708471

A Parametric Study of a Portable Magnetic Separator for Separation of Nanospheres from Circulatory System

Danny Bockenfeld[a]; Haitao Chen[b]; Michael D. Kaminski[c]; Axel J. Rosengart[d]; Dietmar Rempfer[a]
[a] Department of Mechanical, Material and Aerospace Engineering, Illinois Institute of Technology, Chicago, IL, USA [b] Maroon Biotech Corp, Chicago, IL, USA [c] Chemical Sciences and Engineering Division, Argonne National Laboratory, Argonne, IL, USA [d] Department of Neurology and Neuroscience, New York Presbyterian Hospital-Cornell University, NY, USA

Online publication date: 12 February 2010

To cite this Article Bockenfeld, Danny , Chen, Haitao , Kaminski, Michael D. , Rosengart, Axel J. and Rempfer, Dietmar(2010) 'A Parametric Study of a Portable Magnetic Separator for Separation of Nanospheres from Circulatory System', Separation Science and Technology, 45: 3, 355 — 363
To link to this Article: DOI: 10.1080/01496390903485013
URL: http://dx.doi.org/10.1080/01496390903485013

Separation Science and Technology, 45: 355–363, 2010

ISSN: 0149-6395 print/1520-5754 online
DOI: 10.1080/01496390903485013

Taylor & Francis
Taylor & Francis Group

A Parametric Study of a Portable Magnetic Separator for Separation of Nanospheres from Circulatory System

Danny Bockenfeld,[1] Haitao Chen,[2] Michael D. Kaminski,[3] Axel J. Rosengart,[4] and Dietmar Rempfer[1]

[1]*Department of Mechanical, Material and Aerospace Engineering, Illinois Institute of Technology, Chicago, IL, USA*
[2]*Maroon Biotech Corp, Chicago, IL, USA*
[3]*Chemical Sciences and Engineering Division, Argonne National Laboratory, Argonne, IL, USA*
[4]*Department of Neurology and Neuroscience, New York Presbyterian Hospital-Cornell University, NY, USA*

A portable magnetic separator was proposed for *in-vivo* biomedical applications. In this prototype design, a matrix of alternating, parallel magnetizable wires, and biocompatible tubing is immersed into an externally applied magnetic field. The wires are magnetized and high magnetic fields as well as field gradients are created to trap blood-borne flowing magnetic nanospheres in the tube. In this paper, a parametric investigation was carried out to evaluate the capture efficiency of flowing magnetic nanospheres by a separator unit consisting of single tubing and four wires. The parameters include: mean blood velocity (1 to 20 cm/s); magnetic field strength (0.1 to 2.0 T); sphere size (500 nm to 1000 nm in radii); sphere magnetic material (iron, two types of magnetite) and magnetite content in the spheres (0.05 to 0.8 by weight); wire material (nickel, stainless steel 430, and Wairauite); wire length (2.0 to 20 cm); wire size (0.125 to 1.0 mm in radii); tubing size at a fixed ratio of tubing to wire diameter of unity. The results show that capture efficiencies of the spheres of well over 90% were achievable under reasonable human physiological conditions, provided that the mean blood velocities were below about 5.0 cm/s. The results also show that the magnetic separator performance could be improved by maximizing the applied magnetic field strength up to about 1.0 T and by reducing the size of the unit with tubing and wires of equal radii. The results help further optimize a prototype magnetic separator suitable for rapid sequestration of magnetic nanospheres from the human blood stream while accommodating necessary clinical boundary conditions.

Keywords blood filter; magnetic carriers; magnetic filter; magnetic modeling; magnetic separation; magnetic separator; targeted drug therapy

INTRODUCTION

In-vivo biomedical applications for magnetic nano-/micro-spheres have been widely explored because of the potential to direct or concentrate the spheres in target organs or cells. Examples for such applications include drug targeting and delivery (1–2), medical imaging (3–4), hyperthermia treatment (5–6), and blood detoxification (7). Nevertheless, the existence of residual magnetic spheres in the circulatory system after therapy may carry side effects. For example, in magnetically-aided delivery of the clot buster tissue plasminogen activator (tPA) for the reversal of acutely occluded arteries in patients with acute stroke or heart attacks (8), or the magnetically-supported delivery of cancer therapeutics to tumors, some spheres may escape magnetic fields and flow with blood through the body, which may be harmful to healthy tissues due to high toxic or high biologically active therapeutics loaded into those spheres. Moreover, successful removal of blood-borne toxin-bound magnetic spheres is an indispensable step in a recently proposed blood detoxification approach (7). All of these necessitate the development of a suitable magnetic separator to efficiently remove magnetic spheres from fast blood flow *in-vivo*.

Real-time, magnetic separation in a living organism is distinct, as it demands specific and precise design requirements with respect to the human physiology and its proposed medical applications. Different from the magnetic filters in other proposed magnetic extracorporeal units for removing medical agents from body fluids (9–10), which focused on increasing the magnetic field strength in the separators and did not emphasize portability, the filter recently proposed is designed around portability to facilitate in-field use (7). The basic design of this prototype magnetic separator consists of an array of alternating capillary tubing and magnetizable wires which is immersed in a magnetic field generated from two parallel and opposite permanent magnets. The external field is perpendicular to the wires and blood flow. The high magnetic field and high field gradients created by the magnetized wires promote

Received 10 July 2009; accepted 29 October 2009.
Address correspondence to Dietmar Rempfer, Ph.D., Department of Mechanical, Materials & Aerospace Engineering, 10 West 32nd Street, 243 Engineering 1 Building, Chicago, IL 60616-3793. Tel.: 1.312.567.3175; Fax: 1.312.567.7230.

the collection of the magnetic nanospheres from blood flow in the tubing. The design of this prototype portable magnetic separator combines two well-established technologies, the high gradient magnetic separation (HGMS) technique as practiced in industry and laboratory, and the biomedical use of extracorporeal blood circulation, which is the temporary removal and immediate return of blood from and back to the body such as used in hemodialysis for patients with failing kidneys (11). However, in contrast to hemodialysis and similar clinical procedures, no direct blood manipulation is required in this magnetic separation process. Hence, the primary device features include design strategies for ambulatory usage (i.e., light weight, zero power, etc.) (7).

A three-dimensional mathematical model was developed to investigate wire-tubing configuration effects on the capture efficiency (CE) of the device (12). An optimal configuration, in which the wires and the tubing are alternating along both perpendicular and horizontal directions, was preliminarily selected. In this paper, a comprehensive investigation of the effects of various parameters on the CE is performed on this design configuration. The results are used to further optimize the design and the operation of this prototype portable magnetic separator.

MODEL DEVELOPMENT

The finite element package COMSOL Multiphysics 3.3® was used in order to numerically solve the three-dimensional partial differential equations that constitute the model, and to predict the trajectories of the magnetic spheres as they travel with the blood through the tubing while under the influence of both hydrodynamic and magnetic forces (13). In order to reduce the complexity of the model, only one cell of an assumed spatially periodic configuration (see Fig. 1) was used.

The simplicity of the model was achieved by considering only the hydrodynamic (due to the blood flow) and the magnetic forces (due to the effect of the external magnetic field and magnetized wires). Inertial and lift forces, as well as the magnetic interparticle forces that might lead to magnetic sphere agglomeration were neglected. The magnetic sphere trajectory ψ was determined from

$$\nabla \times \psi = \mathrm{u_p}, \tag{1}$$

where $\mathrm{u_p}$ represents the sphere velocity. CE was given by

$$CE(\%) = \left(1 - \frac{n_{\mathrm{p,out}}}{n_{\mathrm{p,in}}}\right) \times 100, \tag{2}$$

where $n_{\mathrm{p,in}}$ is the chosen number of starting points for the magnetic sphere trajectories described by Eq. (1), and $n_{\mathrm{p,out}}$ is the number of trajectories which exit the tubing.

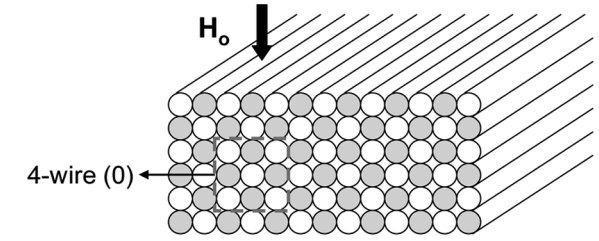

(a)

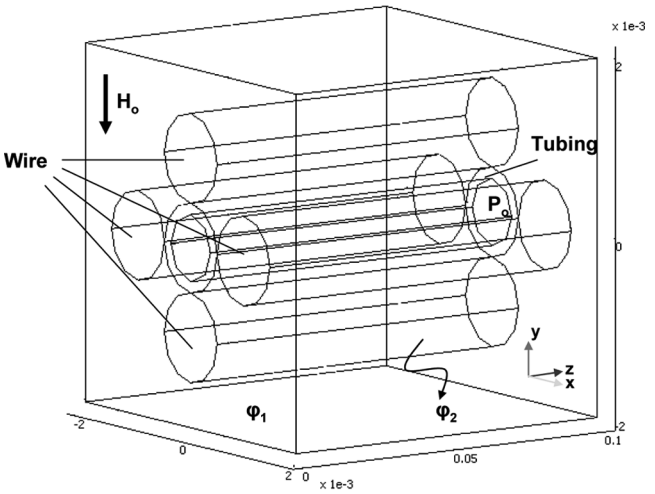

(b)

FIG. 1. (a) The selected configuration design of the magnetizable wires (dark-colored) and tubing (light-colored) in the separator. (b) The schematic view of the magnetic separator unit (3-D) investigated in the current study.

To evaluate Eq. (1), however, the variables that help determine u_p must be first evaluated. This can be done by resolving the force balance that includes hydrodynamic and magnetic forces upon a single magnetic sphere everywhere inside the tubing. These two types of forces were independently evaluated as follows.

First, the blood velocity u and the blood pressure P were found within the tubing by solving the continuity and 3-D Navier-Stokes equations for blood, which was assumed to be an incompressible fluid of density ρ_{B} and viscosity η_{B},

$$\nabla \cdot \mathrm{u} = 0, \tag{3}$$

$$\rho_{\mathrm{B}}\left[\frac{\partial \mathrm{u}}{\partial t} + (\nabla \mathrm{u}) \cdot \mathrm{u}\right] = -\nabla P + \eta_{\mathrm{B}} \nabla^2 \mathrm{u}. \tag{4}$$

The blood flow velocity was assumed to enter the tubing at $z = 0$ in a direction parallel to the tubing walls (i.e., $\mathrm{u_x} = 0$ and $\mathrm{u_y} = 0$) and with a parabolic profile with average velocity U_{o}. At the wall of the tubing, the velocity in all directions was identically zero and at the outlet of the tubing the blood pressure was specified as $P_{\mathrm{o}} = 1$ atm.

Next, the magnetic force upon the magnetic sphere was determined by evaluating the magnetic field H within the CV. This was done using the Maxwell equation within the CV

$$\nabla^2\varphi = 0, \tag{5}$$

where φ is the scalar magnetic potential and is related to the field H according to:

$$\mathrm{H} = -\nabla\varphi. \tag{6}$$

However, the system is composed of two regions with very distinct magnetic behavior. The first region corresponds to the non-magnetic space outside of the wires; the second region corresponds to the space occupied by the wires, which is magnetizable in the presence of an external magnetic field. The discrete nature of the system requires that the magnetic potential be defined differently for each of the regions as φ_1, and φ_2, respectively. Thus, the Maxwell equation is redefined as

$$\nabla^2\varphi_1 = 0, \tag{7a}$$

$$\nabla^2\varphi_2 = 0, \tag{7b}$$

with the respective H being

$$\mathrm{H}_1 = \left(H_{1,\mathrm{x}}, H_{1,\mathrm{y}}, H_{1,\mathrm{z}}\right) = \left(-\frac{\partial\varphi_1}{\partial x}, -\frac{\partial\varphi_1}{\partial y} + H_o, -\frac{\partial\varphi_1}{\partial z}\right), \tag{8a}$$

$$\mathrm{H}_2 = \left(H_{2,\mathrm{x}}, H_{2,\mathrm{y}}, H_{2,\mathrm{z}}\right) = \left(-\frac{\partial\varphi_2}{\partial x}, -\frac{\partial\varphi_2}{\partial y} + H_\mathrm{o}, -\frac{\partial\varphi_2}{\partial z}\right). \tag{8b}$$

On the other hand, the respective magnetic fluxes were defined as

$$\mathrm{B}_1 = \mu_\mathrm{o}(H_{1,\mathrm{x}}, H_{1,\mathrm{y}}, H_{1,\mathrm{z}}) = \mu_\mathrm{o}\left(-\frac{\partial\varphi_1}{\partial x}, -\frac{\partial\varphi_1}{\partial y} + H_\mathrm{o}, -\frac{\partial\varphi_1}{\partial z}\right), \tag{9a}$$

$$\begin{aligned}\mathrm{B}_2 &= \mu_\mathrm{o}(H_{2,\mathrm{x}}, H_{2,\mathrm{y}} + M_\mathrm{w}, H_{2,\mathrm{z}}) \\ &= \mu_\mathrm{o}\left(-\frac{\partial\varphi_2}{\partial x}, -\frac{\partial\varphi 2}{\partial y} + H_\mathrm{o} + M_\mathrm{w}, -\frac{\partial\varphi_2}{\partial z}\right),\end{aligned} \tag{9b}$$

where M_w corresponds to the magnetization in the wires (i.e., region 2). This magnetization is assumed parallel to H_1 and their relationship is defined as

$$|\mathrm{M}_\mathrm{w}| = 2\alpha_\mathrm{w}H_\mathrm{o}, \tag{10a}$$

$$\alpha_w = \min\left(\frac{\chi_{\mathrm{w,o}}}{2+\chi_{\mathrm{w,o}}}, \frac{M_\mathrm{ws}}{2H_\mathrm{o}}\right), \tag{10b}$$

where $\chi_{\mathrm{w,o}}$ and M_ws are the magnetic susceptibility at zero magnetic field and the saturation magnetization of the wires, respectively.

To solve Eq. (7), continuity conditions were applied for the magnetic potential (i.e., φ_1, and φ_2) and the normal components of the magnetic fluxes (i.e., $\mathrm{B}_{1,\mathrm{n}}$, and $\mathrm{B}_{2,\mathrm{n}}$) at every interface between the two defined regions.

In addition, the CV was assumed sufficiently large to impose $\varphi_2 = 0$ along its boundaries. The following expression was then used to evaluate the magnetic force (F_m) on a magnetic sphere:

$$\mathrm{F}_\mathrm{m} = \frac{1}{2}\omega_{\mathrm{fm,p}}V_\mathrm{p}\mu_\mathrm{o}\frac{M_{\mathrm{fm,p}}}{H_1}\nabla(\mathrm{H}_1\cdot\mathrm{H}_1), \tag{11}$$

where μ_o is the magnetic permeability of vacuum, V_p is the volume of the magnetic spheres, and $\omega_{\mathrm{fm,p}}$ and $M_{\mathrm{fm,p}}$ were the volumetric fraction and magnetization of the ferromagnetic material in the magnetic spheres, respectively.

The magnetization of the material in the spheres $M_{\mathrm{fm,p}}$ is assumed parallel to the field H_1. Because the ferromagnetic material in each magnetic sphere is assumed to consist of fully dispersed, single domain, spherical magnetic particles of radius R_sdp, the relationship between the magnetization $M_{\mathrm{fm,p}}$ and H_1 is assumed to follow Langevin's law,

$$M_{\mathrm{fm,p}} = M_{\mathrm{fm,s}}\left[\coth\left(\frac{\mu_\mathrm{o}M_{\mathrm{fm,s}}V_\mathrm{sdp}\left(H_1 - \frac{1}{3}\omega_{\mathrm{fm,p}}M_{\mathrm{fm,p}}\right)}{k_\mathrm{b}T}\right) - \frac{k_\mathrm{b}T}{\mu_\mathrm{o}M_{\mathrm{fm,s}}V_\mathrm{sdp}\left(H_1 - \frac{1}{3}\omega_{\mathrm{fm,p}}M_{\mathrm{fm,p}}\right)}\right], \tag{12}$$

where $M_{\mathrm{fm,s}}$ is the saturation magnetization of the ferromagnetic material inside the magnetic sphere, V_sdp is the volume of a single magnetic particle inside the sphere, k_b is the Boltzman constant and T is the absolute temperature. The term, $1/3\omega_{\mathrm{fm,p}}M_{\mathrm{fm,p}}$, accounts for the demagnetization field due to the magnetic sphere as a whole. For simplicity, however, this term is neglected, mainly due to the small volume fraction $\omega_{\mathrm{fm,p}}$ occupied by the ferromagnetic particles inside a magnetic sphere.

If $\rho_{\mathrm{fm,p}}$ represents the density of the ferromagnetic material inside the magnetic sphere and $\rho_{\mathrm{pol,p}}$ represents the density of the polymer and drug solution comprising the rest of the magnetic sphere, then

$$\omega_{\mathrm{fm,p}} = \rho_\mathrm{p}\frac{\mathrm{f}_{\mathrm{fm,p}}}{\rho_{\mathrm{fm,p}}}, \tag{13}$$

$$\rho_\mathrm{p} = \frac{1}{\frac{\mathrm{f}_{\mathrm{fm,p}}}{\rho_{\mathrm{fm,p}}} + \frac{1-\mathrm{f}_{\mathrm{fm,p}}}{\rho_{\mathrm{pol,p}}}}, \tag{14}$$

where ρ_p is the density of magnetic sphere and $f_{\mathrm{fm,p}}$ is the fraction of magnetic material by weight.

With the expressions for the hydrodynamic forces,

$$\mathrm{F_d} = 6\pi\eta_\mathrm{B} R_\mathrm{p}(\mathrm{u} - \mathrm{u_p}), \tag{15}$$

and magnetic forces (Eq. (11)) defined, Newton's second law of motion for a magnetic sphere, i.e., $\mathrm{F_m} + \mathrm{F_d} = 0$, was finally used to obtain an explicit expression for the magnetic sphere velocity $\mathrm{u_p}$,

$$\mathrm{u_p} = \mathrm{u} + \frac{1}{9}\frac{\mu_\mathrm{o} R_\mathrm{p}^2 \omega_\mathrm{fm,p}}{\eta_\mathrm{B}} \frac{M_\mathrm{fm,p}}{H_1} \nabla(\mathrm{H_1} \cdot \mathrm{H_1}), \tag{16}$$

which follows from equating the Stokes drag of our magnetic particle (Eq. (15)) with the magnetic force.

The components of the magnetic sphere velocity are

$$u_\mathrm{p,x} = u_\mathrm{x} + \frac{V_\mathrm{m} R_\mathrm{w}}{U_\mathrm{o} M_\mathrm{w} H_1}\left(\frac{\partial\varphi_1}{\partial x}\frac{\partial^2\varphi_1}{\partial x^2} + \left(\frac{\partial\varphi_1}{\partial y} - H_\mathrm{o}\right)\frac{\partial^2\varphi_1}{\partial x\partial y} + \frac{\partial\varphi_1}{\partial z}\frac{\partial^2\varphi_1}{\partial x\partial z}\right), \tag{17a}$$

$$u_\mathrm{p,y} = u_\mathrm{y} + \frac{V_\mathrm{m} R_\mathrm{w}}{U_\mathrm{o} M_\mathrm{w} H_1}\left(\frac{\partial\varphi_1}{\partial x}\frac{\partial^2\varphi_1}{\partial x\partial y} + \left(\frac{\partial\varphi_1}{\partial y} - H_\mathrm{o}\right)\frac{\partial^2\varphi_1}{\partial y^2} + \frac{\partial\varphi_1}{\partial z}\frac{\partial^2\varphi_1}{\partial y\partial z}\right), \tag{17b}$$

$$u_\mathrm{p,z} = u_\mathrm{z} + \frac{V_\mathrm{m} R_\mathrm{w}}{U_\mathrm{o} M_\mathrm{w} H_1}\left(\frac{\partial\varphi_1}{\partial x}\frac{\partial^2\varphi_1}{\partial x\partial z} + \left(\frac{\partial\varphi_1}{\partial y} - H_\mathrm{o}\right)\frac{\partial^2\varphi_1}{\partial y\partial z} + \frac{\partial\varphi_1}{\partial z}\frac{\partial^2\varphi_1}{\partial z^2}\right), \tag{17c}$$

where V_m, the so-called magnetic velocity, is given by

$$V_\mathrm{m} = \frac{1}{9}\frac{R_\mathrm{p}^2}{R_\mathrm{w}}\frac{\mu_\mathrm{o}}{\eta_\mathrm{B}}\omega_\mathrm{fm,p} M_\mathrm{fm,p} \cdot M_\mathrm{w}, \tag{18}$$

where R_w is the wire radius.

EXPERIMENTAL CONDITIONS

Based on preliminary calculations in a previous study (12), the baseline conditions of this modeling study were set to be the following: the tubing had an outer radius (R_o) of 0.500 mm, an inner radius (R_i) of 0.375 mm and a length (L_t) of 100 mm; the wires were stainless steel (SS) type 430 with a radius (R_w) of 0.500 mm and a length (L_w) of 100 mm; the magnetic spheres had a radius (R_p) of 200 nm and contained 60 wt% magnetite ($f_\mathrm{fm,p}$); a homogenous magnetic field ($\mu_\mathrm{o}H_\mathrm{o}$) of 0.5 T was applied; the mean blood flow velocity (U_o) through the tubing was 5.0 cm/s. The ranges of the parameters used in the modeling are listed in Table 1, and Table 2 provides other physical and magnetic properties required in this modeling study. The three materials evaluated were iron (saturation

TABLE 1
Values and ranges of the parameters used in the model[a]

Parameters	Units	Values
Fluid density, ρ	kg/m^3	1000
Fluid viscosity, η	kg/(m s)	3.0×10^{-3}
Fluid temperature, T	K	298.15
Mean fluid velocity, U_o	cm/s	1.0–20.0, 5.0
Tube inner radius, R_i	mm	0.150, 0.225, 0.375, 0.750
Tube outer radius, R_o	mm	0.200, 0.300, 0.500, 1.000
Tube length, L_t	mm	20, 50, 100
Sphere radius, R_p	nm	50, 100, 200, 500, 1000
Sphere material[b]		weaker magnetite, magnetite, Fe
Particle radius, R_fm	nm	5
Sphere ferromagnetic mass fraction, $f_\mathrm{fm,p}$		0.05, 0.20, 0.40, 0.60, 0.80
Sphere polymer density, ρ_pol	kg/m^3	950
Wire material[b]		Ni, SS 430, wairauite
Wire radius, R_w	mm	0.250, 0.375, 0.500, 1.000
Wire length, L_w	mm	20, 50, 100, 200
Magnetic field flux density, $\mu_\mathrm{o}H_\mathrm{o}$	T	0.1–2.0, 0.5

[a]Baseline conditions underlined.
[b]Properties indicated in Table 2.

TABLE 2
Physical properties of ferromagnetic materials used in the models

Material	$\rho_{fm,p}$ or ρ_w (kg/m^3)	$M_{w,s}$ or $M_{fm,s}$ (kA/m)
Iron[a]	7850	1735
Typical magnetite[a]	5050	450
Hypothetical weaker magnetite[a]	5050	150
Stainless steel 430[b]	–	1365
Nickel[b]	–	490
Wairauite (CoFe)[b]	–	1922

[a]Magnetic material in the magnetic sphere.
[b]Magnetic material of the wire.

magnetization $M_s = 1735\,\text{kA/m}$), weak magnetite ($M_s = 450\,\text{kA/m}$) and magnetite ($M_s = 150\,\text{kA/m}$). Nickel, SS 430 and Wairauite (a type of CoFe alloy) were investigated as potential wire materials (see Table 2 for values of the saturation magnetization).

RESULTS AND DISCUSSION

An optimal magnetic separator design should achieve high magnetic field density (H) as well as high magnetic field gradient (∇H) in order to efficiently separate flowing magnetic spheres. Though the design only had moderate magnetic field in the separation tubing, it had relatively high magnetic field gradients (Fig. 2). Moreover, it is predictable that the magnetic spheres will experience the repulsive forces from the wires on the left and right sides of the tubing and the attractive forces from the wires on the top and bottom. This prediction is verified when looking at the trajectories of the particles (Fig. 3). Through the trajectories, it can be seen that the particles tend to move towards the wall of the tubing along the y-direction where the attractive forces lie (Fig. 3b), while they tend to move away from the wall of the tubing along the x-direction where the repulsive forces reside (Fig. 3c).

The systematic parametric study varied some of the base parameters in the model, while keeping all the other parameters fixed at the baseline conditions unless otherwise noted. The baseline conditions chosen for this study were considered to be reasonable for the design of a portable

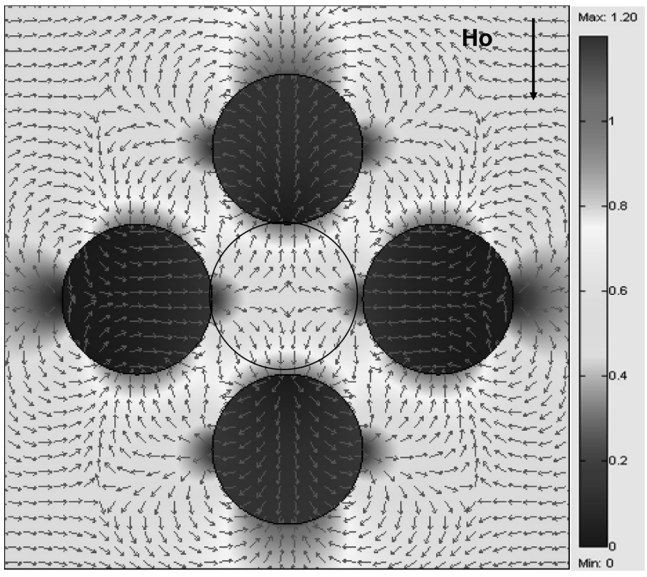

FIG. 2. Typical *COMSOL Multiphysics* simulation results of the magnetic field density through a cross sectional area of the separator units. The coloration indicates the intensity of the magnetic field density and the arrows indicate the direction of magnetic force.

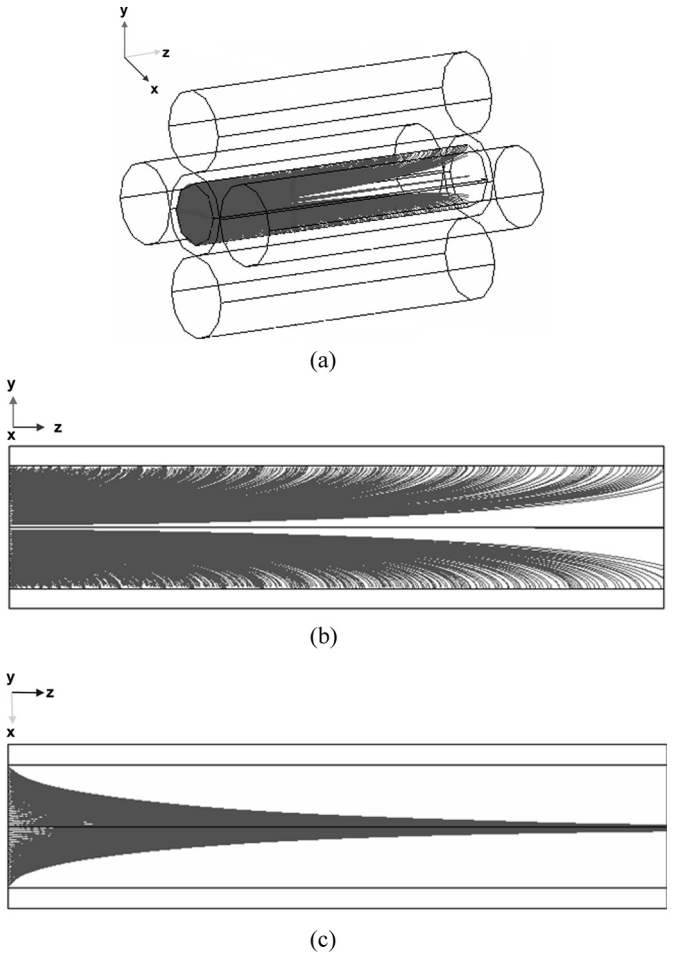

FIG. 3. The trajectories of magnetic spheres at the case of a 4-wire configuration and (a) 3-D and on the planes of (b) $x = 0$ and (c) $y = 0$. Conditions: Tubing: length $L_t = 10\,\text{cm}$, inner diameter $R_i = 0.375\,\text{mm}$ and outer diameter $R_o = 0.50\,\text{mm}$; wires: stainless steel 430 with $L_w = 10\,\text{cm}$ and $R_w = 0.50\,\text{mm}$; spheres: diameter $D_p = 400\,\text{nm}$ containing 60% (by weight) magnetite; fluid: viscosity $\eta = 3.0\,\text{cp}$; applied magnetic field $\mu_o H_o = 0.5\,\text{T}$.

magnetic separator for *in-vivo* blood detoxification described in our previous publications (7,12).

Three-dimensional capture efficiencies were calculated from the sphere trajectories, as noted in Eq. (2). This study focused on the effect of changing flow and field parameters, the magnetic materials, and the physical geometry of the system. By directly modifying the flow and field parameters, important observations can be made. It is not surprising to see that CE decreased with U_o and increased with $\mu_o H_o$ (Fig. 4). However, it is important to notice that the model exhibited no further increase in CE when $\mu_o H_o$ was over 1.0 T. This indicates that a moderate applied magnetic field would be sufficient for this separation system. This was due to the magnetization of the magnetic spheres as well as the magnetizable wires, which will be emphasized later. Moreover, mean flow velocity is an important negative factor. When $U_o = 20\,\text{cm/s}$, CE would be no more than 50% even if $\mu_o H_o = 2.0\,\text{T}$. Therefore, in order to get a desired CE, for example, CE $\geq 90\%$, for one-pass operation, U_o is limited to less than 10 cm/s, for the base conditions.

Another important consideration is the material effect of the magnetic spheres and wires on CE. It is not surprising that spheres with higher magnetite mass content have larger CE (Fig. 5). However, a considerable CE was still predicted even at $f_{fm,p} = 0.05$, being 43.4% and 20.4% at 1.0 cm/s and 5.0 cm/s mean flow velocities, respectively. However, when $f_{fm,p}$ increased from 0.05 to 0.80, CE increased by a factor of two at 1.0 cm/s and by a factor of five at 20 cm/s. However, in order to attain a CE $> 90\%$ in this separation system, the mean flow velocity in each tubing had to be controlled to a low value, e.g., $U_o <$ 5.0 cm/s, or the spheres must have high magnetite content as suggested in the figure. However, too much magnetite can cause toxicity to the human body. Also, very high magnetite content may severely affect the morphology of the spheres such as rough surface and irregular shape (14), which leads to short *in-vivo* circulation life of those spheres.

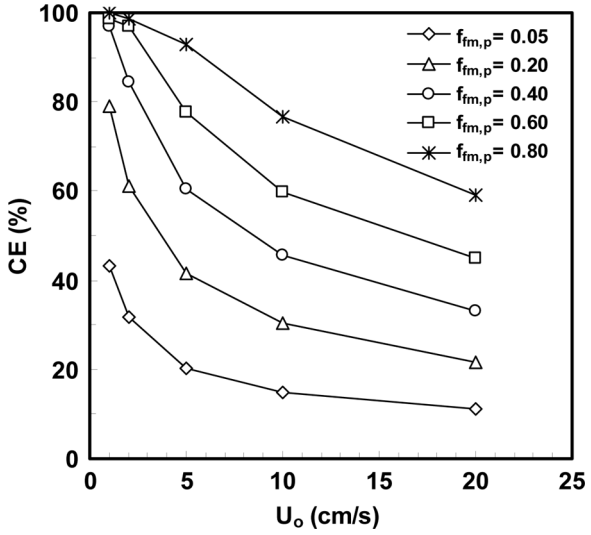

FIG. 5. Effect of magnetite mass content on CE.

The effect of the magnetic material in the magnetic spheres on the CE is shown in Fig. 6. The three materials evaluated were iron (saturation magnetization $M_s =$ 1735 kA/m), weak magnetite ($M_s = 450$ kA/m) and magnetite ($M_s = 150$ kA/m). At $U_o = 5.0\,\text{cm/s}$, increasing CEs of 50%, 78%, and 97.4% are achieved with weaker magnetite, typical magnetite and iron, respectively. Clearly, compared with commonly used iron oxides like magnetite,

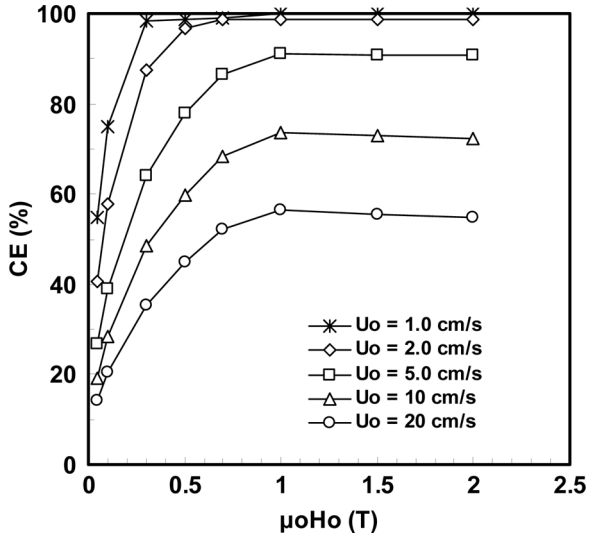

FIG. 4. Effect of flow velocities and applied magnetic field intensity on the CE of the magnetic spheres.

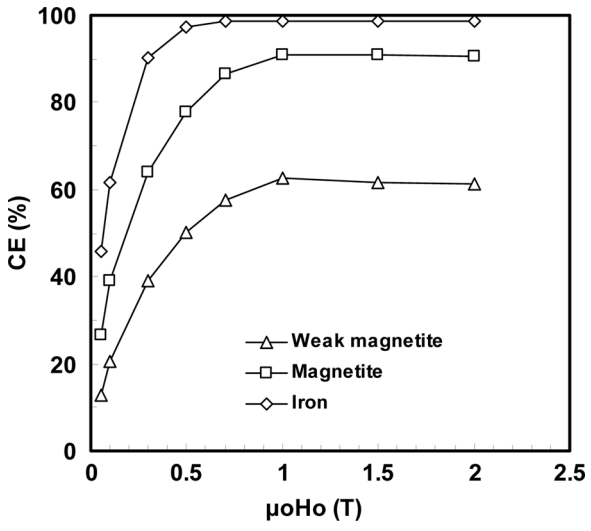

FIG. 6. Effect of the sphere magnetic material on the CE of the magnetic spheres with CE plotted as a function of applied magnetic field intensity.

stronger ferromagnetic materials such as Fe or other equally magnetic metals or alloys are more advantageous. For example, using magnetic spheres containing Fe allows the separator to achieve CE > 90% even at $U_o = 8\,\text{cm/s}$. Of note, unlike the wire materials and model predictions for magnetic particles reported elsewhere (15), these different materials do not exhibit identical behaviors at low magnetic fields. This result is a consequence of Langevin's relationship in Eq. (12) and the magnetic particles within the magnetic spheres are assumed to consist of dispersed single domains. Therefore, their magnetic behavior is no longer controlled by demagnetization effects as reported earlier (15).

The wire material also plays an integral role in CE (Fig. 7). Before reaching the saturation point for nickel ($M_{ws} = 490\,\text{kA/m}$), which is about 0.30 T, all three materials are magnetically unsaturated and thus they display identical magnetic behavior (Fig. 7). However, after this point, nickel is saturated and the CE remains constant at a value of around 63%. Meanwhile, the CEs for SS 430 and wairauite continue to increase together as one curve until the magnetic field reaches 0.7 T. After this point, SS 430 becomes saturated and the CE for it remains constant at about 91% while the CE for wairauite continues to increase until its saturation field of 1.2 T with a CE of around 97%.

There are two important observations from the results. First, magnetic materials display identical behavior in relatively strong magnetic fields (up to 0.30 T) despite their significant differences in magnetic character. For example, the CEs for nickel and Wairauite do not differ until at 0.30 T even though there is a four-fold difference in the saturation magnetizations of these two materials. Another observation is that it is unnecessary to apply a very high magnetic field (>1.2 T) on the magnetic separator unit. At 1.2 T, most ferromagnetic materials of cylindrical shape are already magnetically saturated. Of note, for a human blood detoxification process, wire material with high saturation magnetization is preferable because the strict *ex-vivo* separation task requires high CE (>90%) at a moderate or high flow rate conditions (7). A stainless steel like SS 430 is an ideal candidate for wire material in the device due to its high saturation magnetization and easy availability. In this case, the applied magnetic field would not be larger than 1.0 Tesla.

In addition to the material effects, there are important geometric effects of both the device and the spheres. Figure 8 shows the effect of sphere size on the capture efficiency (CE) of the magnetic spheres. It is apparent that the sphere size D_p is a very important parameter in this system. When D_p increases from 100 nm to 2000 nm, CE increases from 50% to 100% at 1.0 cm/s and from 12.6% to 98.8% at 20 cm/s. For a sphere with a predefined magnetite content, i.e., $f_{fm,p}$ is constant, the magnetic force F_m on the sphere is a function of D_P^3 while the drag force F_d on the sphere is proportional to D_p only. Therefore, increasing sphere size produces greater effect on the magnetic force than it does on the drag force. However, the size of the spheres has to be in a suitable range for detoxification application due to the physiologic characteristics of the human body. If the spheres are too big, they will occlude the capillaries. On the other hand, if the spheres are too small, not only is it difficult to efficiently capture them from blood flow, but also they might be filtered from the circulatory system by the kidneys (16). The spheres with size range of 100 nm to 2000 nm seem suitable for future blood detoxification purposes.

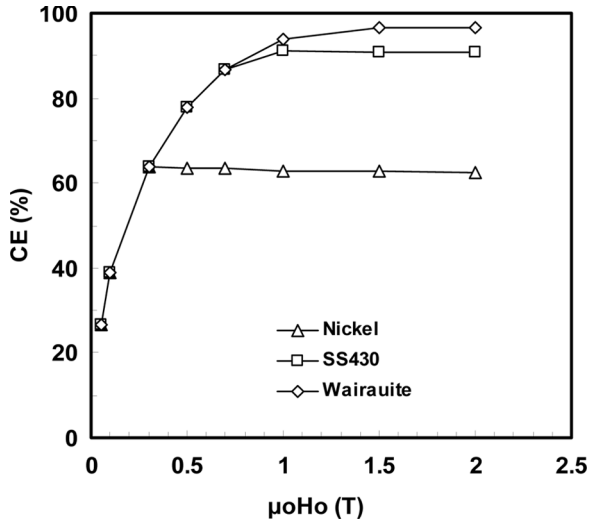

FIG. 7. Effect of the wire material on the CE of the magnetic spheres with CE plotted as a function of applied magnetic field intensity.

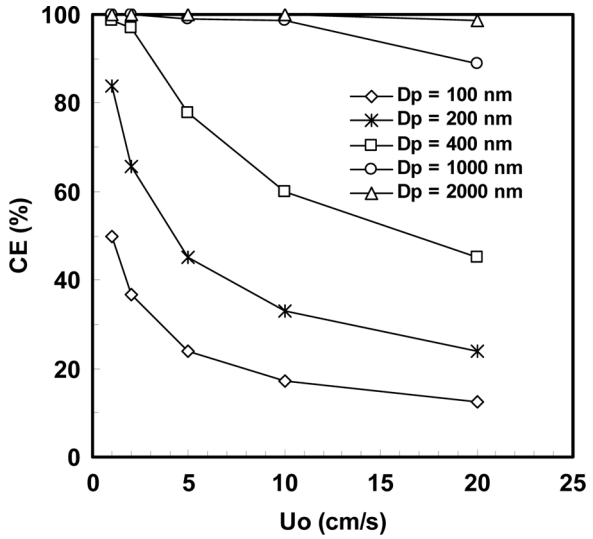

FIG. 8. Effect of sphere size on CE.

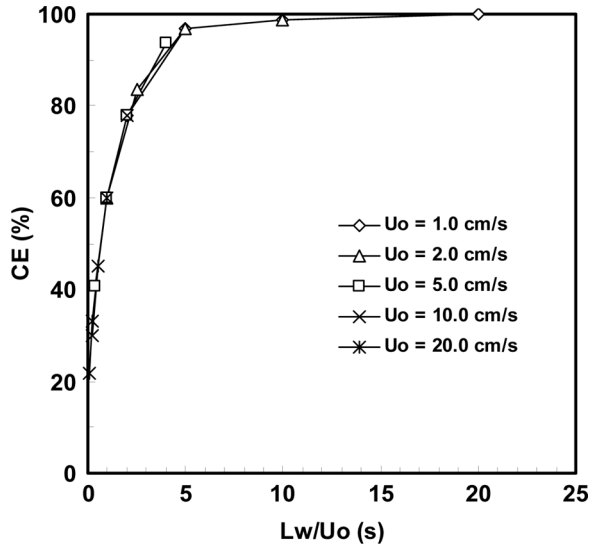

FIG. 9. Effect of the wire length on the CE of the spheres with CE plotted as a function of residence time L_w/U_o for different mean velocities.

Figure 9 shows the effect of the wire length on the CE of the spheres. The results were plotted as a function of the fluid residence time L_w/U_o for different U_o at the base case conditions. The results collapse onto a single curve. The CE improved with increasing L_w, which is due to the longer residence times in the separation area. This indicates that the CE is eventually a function of L_w/U_o and independent mechanic processes control the axial and radial movements of the spheres.

The effect of the wire size on the CE as a function of R_w/R_o is shown in Fig. 10. Generally, as $\mu_o H_o$ increases, CE increases rather sharply at low $\mu_o H_o$ and then more gradually at higher $\mu_o H_o$. Moreover, the CEs range from 22.8% to 26.7% at $\mu_o H_o = 0.05$ T and from 84.9% to 91% at $\mu_o H_o = 1.0$ T, indicating a significant effect of the applied field on the CE. Since the hydrodynamic force is being held constant under these conditions, as $\mu_o H_o$ increases, the magnetic force increases resulting in an increasingly larger imbalance in these forces, which manifests as an increasing CE. However, there is no further noticeable increase in CE when $\mu_o H_o$ exceeds 1.0 T, which is due to the magnetic saturation of the wire materials as well as the magnetic materials in the spheres as stated previously. It is of importance to see that the lowest CE is exhibited by the largest R_w/R_o (=2) in all cases despite the maximum mass of magnetic material available for the biggest wires. The indication from the results in Fig. 10 tells us that the best performance of the device can be expected when $R_w/R_o = 1$. This result clearly reveals the important interaction between the local magnetic field and the local magnetic field gradients. The combination of slightly lower magnetic field and much higher magnetic field gradients from the smaller wires produces the larger magnetic force and therefore higher CE for the separation system.

Aside from modifying the geometry of the wires and spheres, a change in the tubing size also modifies the CE. Figure 11 displays the effect of the outer capillary tube radius (R_o) on the CE of the spheres for the baseline conditions while keeping $R_o/R_w = 1.0$ and $R_i/R_o = 0.75$. One may wonder whether scaling the radii of the wires and tubing together would show a noticeable change in CE. However, the results show that CE benefits from reducing the size of the tube-wire unit. For example, at $U_o = 10$ cm/s, the CE increased from 33% to about 98% when R_o decreased from 1.0 mm to 0.2 mm. This is an interesting and slightly perplexing phenomenon. However,

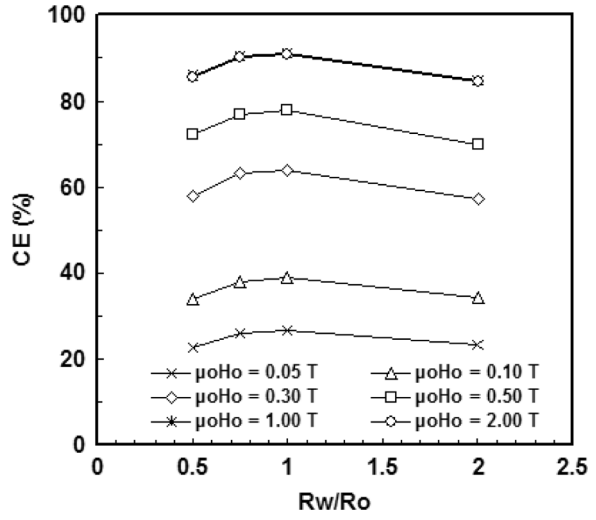

FIG. 10. Effect of the wire radius on the CE of the spheres with CE plotted as a function of wire radius/tube outer radius ratio.

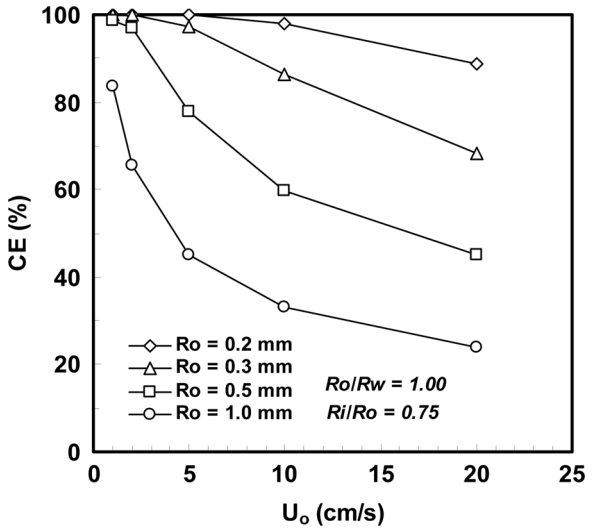

FIG. 11. Effect of the tubing size on the CE of the spheres.

it is a consequence of HGMS effect (15). Smaller wires can produce shorter-ranged magnetic fields as well as higher magnetic field gradients in the adjacent area. It is known from Eq. (11) that the magnetic force is proportional to magnetic field and field gradient. It is the higher magnetic field gradient that gives higher CE for smaller wires in Fig. 11. Apparently, it is advantageous to miniaturize the magnetic separator unit in order to increase the capture efficiency. However, in a practical blood detoxification process, the extent of the miniaturization should be determined by the size and magnetic properties of spheres, the amount of them to be removed, and the volume of the blood to be processed.

CONCLUSION

A parametric investigation was carried out to evaluate the capture efficiency of flowing magnetic spheres by the unit of a prototype magnetic separator for human blood detoxification (Fig. 1b). The results showed that CEs of the spheres of well over 90% were achievable under reasonable human physiological conditions, provided that the mean blood velocities were below about 5.0 cm/s. The results also showed that CEs of the spheres of between 20% and 60% could easily be attained at higher velocity up to 20 cm/s at moderate systemic and operating conditions.

The parametric study showed that the magnetic separator performance could be improved by increasing the size of the spheres and their content of magnetic material while keeping in mind the corresponding detrimental effects of capillary tube occlusion in the device; by utilizing magnetic materials in both the wires and the spheres with the highest magnetizations while taking into consideration the cost, availability, and physico-chemical stability of the materials; by maximizing the applied magnetic field strength up to about 1.0 T; by decreasing the mean flow velocity in the tubing while considering the separation task, i.e., separation time and flow volume; by reducing the size of the unit with tubing and wires of equal radii; and by increasing the length of the separator unit while keeping in mind the corresponding detrimental effects on pressure drop and portability and the cost for materials and device production.

The results further optimize a prototype portable magnetic separator suitable for rapid sequestration of magnetic nanospheres from the human blood stream for human detoxification.

ACKNOWLEDGEMENTS

This work was supported by the University of Chicago, and The University of Chicago Brain Research and the Cancer Research Foundations, Chicago, the Department of Energy under contract DE-AC02-06CH11357, and an ERIF Grant by Illinois Institute of Technology.

REFERENCES

1. Alexiou, C.; Arnold, W.; Hulin, P.; Klein, R.J.; Renz, H.; Parak, F.G.; Bergemann, C.; Lubbe, A.S. (2001) Magnetic mitoxantrone nanoparticle detection by histology, X-ray and MRI after magnetic tumor targeting. *J. Magn. Magn. Mater.*, 225: 187.
2. Zhang, Y.Q.; Li, L.L.; Tang, F.Q.; Ren, J. (2006) Controlled drug delivery system based on magnetic hollow spheres/polyelectrolyte multilayer core-shell structure. *J. Nanosci. Nanotechnol.*, 6: 3210.
3. Mulder, W.J.M.; Strijkers, G.J.; Griffioen, A.W.; van Bloois, L.; Molema, G.; Storm, G.; Koning, G.A.; Nicolay, K. (2004) A liposomal system for contrast-enhanced magnetic resonance imaging of molecular targets. *Bioconjugate. Chem.*, 15: 799.
4. Sun, E.Y.; Josephson, L.; Weissleder, R. (2006) "Clickable" nanoparticles for targeted imaging. *Mol. Imaging*, 5: 122.
5. Ito, A.; Shinkai, M.; Honda, H.; Kobayashi, T. (2005) Medical application of functionalized magnetic nanoparticles. *J. Biosci. Bioeng.*, 100: 1.
6. Liu, X.; Novosad, V.; Rozhkova, E.A.; Chen, H.; Yefremenko, V.; Pearson, J.; Torno, M.; Bader, S.D.; Rosengart, A.J. (2007) Surface functionalized biocompatible magnetic nanospheres for cancer hyperthermia. *IEEE Trans. Magn.*, 43: 2462.
7. Chen, H.; Kaminski, M.D.; Liu, X.; Mertz, C.J.; Xie, Y.; Torno, M.D.; Rosengart, A.J. (2007) A novel human detoxification system based on nanoscale bioengineering and magnetic separation techniques. *Med. Hypotheses*, 68: 1071.
8. Rosengart, A.J.; Chen, H.; Xie, Y.; Kaminski, M.D. (2005) Magnetically guided plasminogen activator-loaded designer spheres for acute stroke lysis. *Med. Hypotheses Res.*, 2: 413.
9. Gordon, L.S. (2003) Magnetic extracorporeal circuit for removal of medical agents. US Patent, US0120202/2003.
10. Carew, B. (1992) Method for separating pathogenic or toxic agents from a body fluid and return to body. US Patent, US5123901/1992.
11. Swartz, R.D.; Somermeyer, M.G.; Hsu, C.H. (1982) Preservation of plasma-volume during hemodialysis depends on dialysate osmolality. *Am. J. Nephrol.*, 2: 189.
12. Chen, H.; Bockenfeld, D.; Rempfer, D.; Kaminski, M.D.; Rosengart, A.J. (2007) Three-dimensional modeling of a portable medical device for magnetic separation of particles from biological fluids. *Phys. Med. Biol.*, 52: 5205.
13. Ritter, J.A.; Ebner, A.D.; Daniel, K.D.; Stewart, K.L. (2004) Application of high gradient magnetic separation principals to magnetic drug targeting. *J. Magn. Magn. Mater.*, 280: 184.
14. Liu, X.; Kaminski, M.D.; Chen, H.; Torno, M.; Taylor, L.; Rosengart, A.J. (2007) Synthesis and characterization of highly-magnetic biodegradable poly(D,L-lactide-co-glycolide) nanospheres. *J. Control Release*, 119: 52.
15. Chen, H.; Ebner, A.D.; Kaminski, M.D.; Rosengart, A.J.; Ritter, J.A. (2005) Analysis of magnetic drug carrier particle capture by a magnetizable intravascular stent-2: Parametric study with multi-wire two-dimensional model. *J. Magn. Magn. Mater.*, 293: 616.
16. Gref, R.; Minamitake, Y.; Peracchia, M.T.; Trubetskoy, V.; Torchilin, V.; Langer, R. (1994) Biodegradable long-circulation polymeric nanospheres. *Science*, 263: 1600.